ACI STRUCTURAL JOURNAL TECHNICAL PAPER

Title no. 102-S79

Seismic Resistance of Square Concrete Columns Retrofitted with Glass Fiber-Reinforced Polymer

by Muhammad S. Memon and Shamim A. Sheikh

The capacity of key structural members, particularly columns, to absorb and dissipate energy without severe strength degradation dictates the survival of structures during a major earthquake. Reinforced concrete columns with inadequate confinement do not possess the necessary ductility to dissipate sufficient seismic energy. This research evaluates the effectiveness of glass fiber-reinforced polymer (GFRP) wraps in strengthening deficient and repairing damaged square concrete columns. Each of the eight specimens tested, representing columns of buildings and bridges constructed before 1971, consisted of a 305 x 305 x 1473 mm column connected to a 508 x 762 x 813 mm stub. Specimens were tested under constant axial compression and cyclic lateral displacement excursions simulating earthquake loads. Test results reveal that retrofitting with GFRP wraps significantly enhanced ductility, energy dissipation ability, and shear and moment capacities of deficient columns. Cyclic behavior progressively improved as the number of GFRP layers increased, causing both stiffness degradation and strength reduction rates to decrease. Improvements observed following GFRP repair of damaged columns depended mainly on the extent of damage sustained. GFRP-confined columns exceeded the performance of similar columns that contained transverse steel reinforcement in accordance with the seismic provisions of the current North American codes.

Keywords: column; concrete; confinement; ductility; repair; seismic.

INTRODUCTION

The ability of structures to withstand severe earthquake vibrations and to perform in a satisfactory manner in post-elastic states depends mainly on the formation of plastic hinges and their capacity to absorb and dissipate seismic energy. Most building codes[1] provide guidelines to ensure that the seismic energy is dissipated in beams and girders rather than columns. Despite this strong column-weak beam concept, plastic hinging in columns during severe earthquakes is still unavoidable. Hinging of columns at the base of the structure is, in fact, depended upon to develop the mechanism to dissipate energy. Therefore, column performance in the inelastic mode is of utmost importance for the safety of a structure during an earthquake. It is well known that appropriate confinement of the potential plastic hinge regions ensures the ability of columns to sustain inelastic displacement without significant strength and stiffness degradation during severe earthquakes.

An investigation of the damages to buildings and highway structures in recent earthquakes in California and Japan[2,3] has demonstrated the vulnerability of concrete columns, particularly in the structures constructed prior to 1971. The amount of lateral reinforcement used in such columns was as low as 10 to 15% of that specified by the current seismic design codes, thereby putting these structures at risk of rapid failure in a severe earthquake. As a result, major efforts were directed toward developing and applying retrofitting strategies to upgrade such columns. A retrofit technique using glass and carbon fiber-reinforced polymer materials (FRPs) is such an innovation. The advantages of glass FRP (GFRP) over the conventional external confinement techniques (reinforced concrete jacketing and steel plate jacketing) include higher strength-to-weight ratio, greater contact area, increased resistance to corrosion, ease of installation, lower labor and construction costs, and maintenance of the original member stiffness.

In recent years, despite a limited amount of experimental data on the seismic behavior of FRP-confined concrete columns, external FRP systems have become widespread in field column applications. The main objective of this research is to study the effectiveness of strengthening deficiently built columns as well as repairing damaged square columns with GFRP sheets for seismic resistance. The work presented herein is part of a comprehensive research program[4-6] that aims to study the use of FRP to improve the behavior of concrete structures under a variety of extreme loads. Results from a recent test series on GFRP-confined square concrete columns are presented in this paper.

RESEARCH SIGNIFICANCE

A very limited amount of experimental data exists on the seismic behavior of realistically sized square concrete columns confined with GFRP wraps. This research investigates the seismic performance of near full-scale GFRP-retrofitted columns typical of existing buildings and highways. The reported study addresses the repair of damaged columns with GFRP—a topic of significant importance for the construction industry. The seismic responses of GFRP-confined columns are compared with those of similar columns reinforced only with transverse steel in accordance with the ACI code provisions. Results can be used to design retrofitting schemes for deficient columns and also to develop design guidelines for retrofitting with GFRP.

EXPERIMENTAL PROGRAM

Eight large-scale reinforced concrete columns were constructed using typical lateral steel detailing from the pre-1971 design codes. Seven of these columns were strengthened or repaired with GFRP wraps. One unwrapped column from this program and one from an earlier study[6] were used as control specimens to evaluate the benefits of FRP retrofitting. All the

ACI Structural Journal, V. 102, No. 5, September-October 2005.
MS No. 04-335 received October 12, 2004, and reviewed under Institute publication policies. Pertinent discussion including author's closure, if any, will be published in the July-August 2006 *ACI Structural Journal* if the discussion is received by March 1, 2006.

Muhammad S. Memon *is the Chief Project Engineer with Eastern Construction Co. Ltd., Toronto, Ontario, Canada. He received his MASc in 2002 from the University of Toronto, Toronto, Canada. He is a registered professional engineer in Ontario.*

Shamim A. Sheikh, *FACI, is a professor of civil engineering at the University of Toronto. He is a member and Past Chair of Joint ACI-ASCE Committee 441, Reinforced Concrete Columns, and a member of ACI Committee 374, Performance-Based Seismic Design of Concrete Buildings. He received the ACI Structural Research Award in 1999. His research interests include earthquake resistance and seismic upgrade of concrete structures, confinement of concrete, use of fiber-reinforced polymer in concrete structures, and expansive cement and its applications.*

specimens were tested under constant axial load and cyclic lateral excursions simulating seismic loading conditions. The main variables of the study were the number of GFRP layers in the potential plastic hinge region, the level of applied axial load, and the presence of column damage.

Specimens

Each specimen consisted of a square column of dimensions 305 x 305 x 1473 mm cast integrally with a stub of dimensions 508 x 762 x 813 mm. The column represented a portion of a column in a bridge or a building between the section of maximum moment and the point of contraflexure. The stub represented the discontinuity similar to a footing or a beam-column joint. The total core area was approximately equal to 77% of the gross area of the column. All columns contained eight 20M longitudinal bars uniformly distributed around the core. Perimeter ties laterally supported the four corner bars and internal ties enclosed the four middle bars. The corners of columns were rounded to facilitate GFRP wrapping using concave wood sections, with a 16 mm radius, placed inside the forms. Details of the specimens are given in Table 1 and Fig. 1. To differentiate these specimens from others in this extensive program, their designations imply their unique features. The first two letters (AS) represent the configuration depicted in Fig. 1. The letter G stands for glass fiber used in the test. The letter R represents the repaired specimens. NS denotes the normal-strength concrete used, whereas the letter S indicates the presence of stub.

Concrete and grout

The specimens were cast together using a ready mixed concrete design consisting of Type 10 (U.S. Type I) portland cement and 10 mm maximum aggregate size with specified slump of 100 mm and nominal compressive strength of 30 MPa. The stub was first filled with concrete through column formwork and was compacted with rod vibrators. Columns were then cast and vibrated thoroughly. Open surfaces of the specimens were covered with wet burlap and plastic sheets. Thirty 152 x 304 mm cylinders were also cast with column specimens to monitor strength development of concrete with age. The concrete strength at the time of testing of each column is shown in Table 1.

A nonshrink structural grout with aggregate was used for the repair of two specimens (Specimens 7 and 8). A water-cement ratio (w/c) of 0.24 was used to assure adequate workability for placement. Average compressive strength reached 41 and 42 MPa at 7 and 14 days, respectively—approximately equal to the original concrete strengths in the two repaired specimens.

Steel

Three types of steel were used in the construction of the specimens. Longitudinal reinforcement consisted of eight 20M bars, rectilinear and diamond ties were made with U.S. No. 3 bars, and stub stirrups with 10M bars. Properties of steel bars are given in Table 2.

Reinforcing cages and instrumentation

Reinforcing cages for all the specimens consisted of two parts, that is, a cage for the column and a cage for the stub. Both cages were assembled separately and later connected to each other. The column cage consisted of eight 20M diameter longitudinal bars (2248 mm long) uniformly distributed around the core perimeter. The longitudinal steel extended through the stubs to 15 mm from the end. U.S. No. 3 bars were used for ties, with 135-degree hooks, as lateral reinforcement. The test region was within 610 mm of the stub face. The ties were placed at a spacing of 300 mm within the test region. Tie spacing was reduced to 150 mm outside of test region to minimize the chances of failure there. The stub

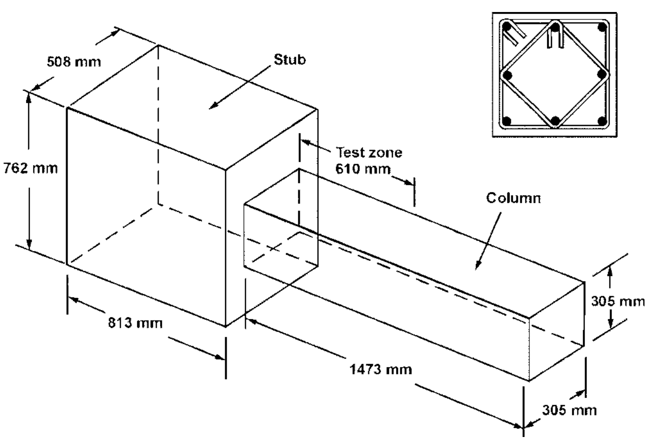

Fig. 1—Geometry and lateral steel configuration of specimens.

Table 1—Details of test specimens

Specimen	f_c', MPa	GFRP treatment	Axial load P/P_o	Lateral steel			Longitudinal steel	
				Size at spacing s, mm	ρ_s, %	$A_{sh}/A_{sh(ACI)}$	No. of bars and size	ρ_g, %
AS-1NSS	42.4	None	0.56	U.S. No. 3 at 300	0.61	0.36	Eight-20M	2.58
ASG-2NSS	42.5	Two layers	0.33	U.S. No. 3 at 300	0.61	0.36	Eight-20M	2.58
ASG-3NSS	42.7	Four layers	0.56	U.S. No. 3 at 300	0.61	0.36	Eight-20M	2.58
ASG-4NSS	43.3	Two layers	0.56	U.S. No. 3 at 300	0.61	0.35	Eight-20M	2.58
ASG-5NSS	43.7	One layer	0.33	U.S. No. 3 at 300	0.61	0.35	Eight-20M	2.58
ASG-6NSS	44.2	Six layers	0.56	U.S. No. 3 at 300	0.61	0.34	Eight-20M	2.58
ASGR-7NSS	44.2	Two layers	0.33	U.S. No. 3 at 300	0.61	0.34	Eight-20M	2.58
ASGR-8NSS	44.2	Six layers	0.56	U.S. No. 3 at 300	0.61	0.34	Eight-20M	2.58
AS-3[9]	33.2	None	0.50	U.S. No. 3 at 108	1.68	1.43	Eight No. 6	2.44
AS-19[9]	32.3	None	0.39	U.S. No. 3/6 mm at 108	1.30	1.12	Eight No. 6	2.44

cage consisted of 10M horizontal and vertical stirrups placed at 64 mm spacing. Additional 10M bars with 135-degree hooks were added at two sides to increase stub stiffness.

Thirty-four electric strain gauges, 18 on the longitudinal bars and 16 on the ties, were installed in every specimen.

Table 2—Mechanical properties of steel bars

Bar type	Diameter, mm	Area, mm^2	Modulus E_s, MPa	Yield stress f_y, MPa	Yield strain ε_y	Ultimate stress f_{ult}, MPa	Ultimate strain ε_{ult}
20M	19.5	300	202,170	465	0.0023	640	0.2021
10M	11.3	100	180,360	505	0.0028	680	0.2151
U.S. No. 3	9.5	71	207,730	457	0.0022	739	0.1411

Table 3—Tensile properties of GFRP composites through coupon tests

No. of GFRP coupons	Average strength, N/mm	Average rupture strain	Maximum strength, N/mm	Maximum rupture strain	Minimum strength, N/mm	Minimum rupture strain
8	563	0.0228	586	0.0242	540	0.0214

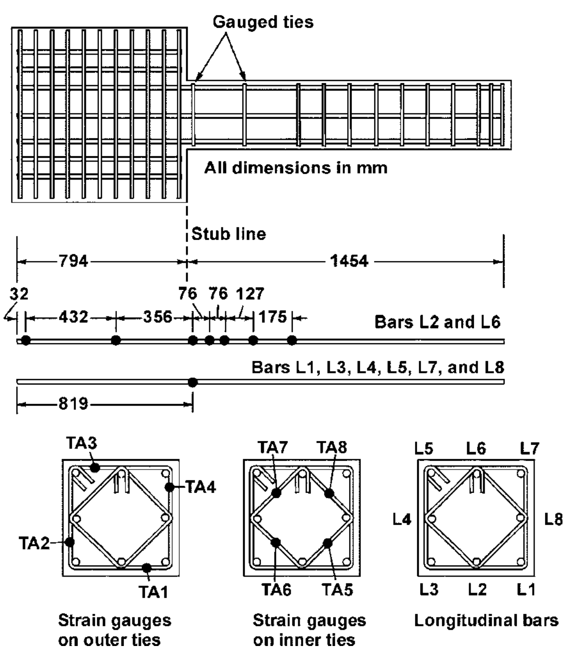

Fig. 2—Location of strain gauges on longitudinal and lateral steel.

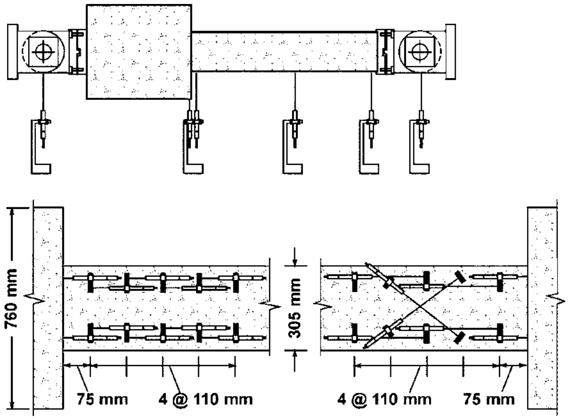

Fig. 3—LVDT arrangement.

Eight longitudinal bars and two sets of lateral ties in each specimen were strain-gauged individually before being assembled to create a column cage. Figure 2 shows the location of strain gauges.

Glass fiber-reinforced polymers

A commercially available GFRP wrap system was used to retrofit the designated specimens. The average thickness of a GFRP laminate was 1.25 mm. The average tensile properties of FRP, as obtained from eight coupon tests, are reported in Table 3.

Prior to applying FRP, the concrete surface was smoothed using sandpaper, and voids, if any, were filled using plaster of paris. Two components (A and B) of polymer materials were mixed to form epoxy for the fiber wrap. Glass fabric was cut to required length depending on the number of FRP layers in the specimen, placed on a plastic sheet and saturated with epoxy using a roller brush. The column surface was then coated with epoxy and the impregnated fabric was tightly wrapped around the column, ensuring that there were no entrapped air pockets or fabric distortions. The fibers were oriented in the lateral direction. A 610 mm-wide fabric sheet was used for the test region while a 915 mm (including 50 mm overlap) wide sheet was wrapped outside of the test zone. An extra layer was wrapped around the column length outside the test region to minimize the possibility of failure there.

To accommodate the threaded rods embedded in the specimens for installing testing instrumentation, openings in GFRP were made by separating the fibers at all rod locations as each layer of FRP was installed. Considering the weakness generated by the presence of these holes, an additional strip of 100 x 585 mm was place to strengthen each of the four lines of embedded rods. GFRP wraps were left for 7 days to cure before testing of specimens.

Specimen instrumentation

Strains in the longitudinal and lateral steel were measured using 34 strain gauges shown in Fig. 2. A total of 18 LVDTs, 10 on north side and eight on south side, were mounted to the embedded rods to measure the deformations of the concrete core in the test region of the specimens (Fig. 3). The gauge lengths for the LVDTs varied from 75 to 220 mm. Deflection along the length of the specimen was measured using six LVDTs, also shown in Fig. 3. Eight surface strain gauges were used to monitor the lateral strains in GFRP. Two gauges were placed on the longitudinal centerline of each column face in the direction of fibers at 130 and 240 mm, respectively, from the stub face.

Testing

The specimens were tested horizontally in the testing frame, as shown in Fig. 4. The axial load was applied through a hydraulic jack having the capacity of 4450 kN and was measured using a load cell of similar capacity. Special hinges were used at the ends of the specimen to allow in-plane rotation and to keep the loading path constant throughout the test. To apply reverse lateral load, an actuator with a load capacity of 1000 kN and a stroke capacity of ±150 mm was used. The displacement control feature of the actuator was used in all the tests to apply predefined displacement history, as shown in Fig. 5. The hinges at both ends of the actuator were adjusted to allow in-plane rotation at the lower end of the actuator.

The specimen was aligned in the vertical plane using engineering levels. In the horizontal plane, plumb-bobs were used to match the centerline of the specimen with the line of action of the axial load. After the external instrumentation was installed, the specimen was loaded up to 50% of the predetermined axial load in 200 kN increments. The deformations at the four corners of the specimen were recorded using four LVDTs. If the difference between the average reading and the maximum or minimum displacement reading was more than 5%, the specimen was unloaded and necessary adjustments were made. The process was repeated until the specimen was properly aligned. The strain gauge readings were also used to confirm the alignment.

The test started with the application of pre-assigned axial load followed by the application of lateral displacement sequence (Fig. 5). The specimen was subjected to 75% of the yield or elastic displacement (Δ_1) in the first cycle; the displacement Δ_1 is also defined in Fig. 5. The displacement Δ_1 was determined from the theoretical section behavior of the column and integrating curvatures along its length. In the subsequent cycles, the lateral excursions were increased gradually (two cycles each to $2\Delta_1$, $3\Delta_1$, $4\Delta_1$ ….) until the specimen was unable to maintain the applied axial load resulting in the termination of the test.

Each of the two specimens chosen to undergo repair was subjected to axial load and lateral displacement excursions until, at minimum, the top and bottom concrete cover spalled off and the yielding of the longitudinal bars initiated. For Specimen ASGR-7NSS subjected to an axial load of 1490 kN, spalling of the top and bottom concrete cover occurred in the sixth cycle. The maximum displacement in the critical region was approximately $2.55\Delta_1$ and the average maximum compressive strain in the longitudinal bars was 0.00258. The amount of damage causing spalling of the concrete cover and yielding of the longitudinal steel was considered appropriate for most columns that are candidates for repair. The specimen was then returned to zero lateral displacement position for repair. For the purpose of safety during the repair process, the axial load was reduced to 66% of the original axial load value. The loose concrete was carefully removed from the damaged column as the repair took place under the applied axial load to simulate the field conditions. Nonshrink grout was used to repair the damaged specimen. After 3 days, when the grout had cured and dried, the specimen was wrapped with GFRP while it remained in the test frame. After the curing of GFRP sheets, the specimen was tested to failure with an axial load of 1490 kN.

The top and bottom concrete cover spalled off and the yielding of longitudinal bars initiated during the third cycle for Specimen ASGR-8NSS while maintaining an axial load of 2500 kN. The average maximum compressive strain in the longitudinal bars was 0.00251. With this damage, the repair of the specimen was carried out under an axial load of approximately 60% of its original value. The same procedure of repair, wrapping, and retesting was adopted as used for Specimen ASGR-7NSS.

RESULTS

Test observations

In all the specimens, the cyclic loading was applied by pushing the specimens at the stub near the column in downward direction first. The first sign of distress in the control Specimen AS-1NSS ($0.56P_o$) appeared in the form of cracks in the cover concrete at the top and the bottom of the column. Vertical flexural cracks formed at distances of 300 to 350 mm from the face of the stub during the first three cycles. The top cover spalled over a distance of 270 mm close to the stub at the peak of fourth cycle downward ($\Delta = 2\Delta_1$). The bottom cover spalled in a 380 mm region during the fourth cycle ($\Delta = 1.56\Delta_1$) upward. Buckling of the longitudinal bars, during the fourth cycle ($\Delta = 1.85\Delta_1$) upward, was observed as an indication of commencement of failure after yielding of lateral steel. Flexure-shear effects dominated the specimen behavior.

The initial occurrence of the cracks and crushing of the concrete cover in the wrapped specimens were not visible. The separation of fibers from the concrete, as indicated by the change in FRP color, however, was observed in all specimens within hinging zones as crushing of concrete started. With the increase in the lateral excursions, the breaking sounds from the hardened epoxy within the hinging zone increased, indicating the severity of the deformation.

At a low axial load level ($0.33P_o$), the specimens showed an almost elastic behavior for the first three cycles in all the tests. In the later cycles, the first sign of the deformation was the formation of the ridges or bumps in GFRP on the top and the bottom surfaces of the specimens in the test region. The ridges mostly initiated at approximately 250 to 310 mm from the column-stub interface. The length and height of the ridges increased as the specimens were subjected to increased cyclic excursions. Most of the damage (observed through popping sounds of hardened epoxy matrix and the formation of ridges) extended initially from 355 mm to approximately 60 mm from stub's interface. The column section adjacent to the stub was subjected to the highest moment but, due to the additional confinement provided by the stub, the damage initiated away from the stub at a

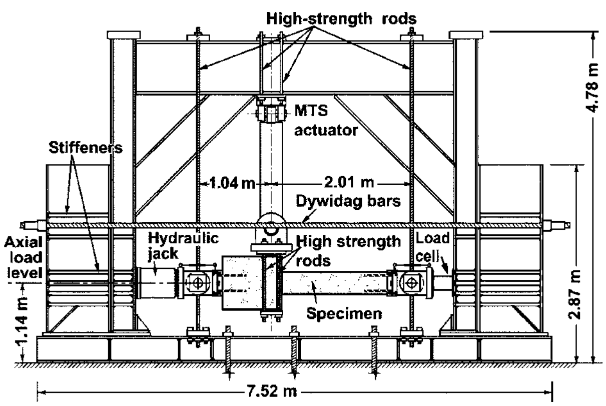

Fig. 4—Testing frame.

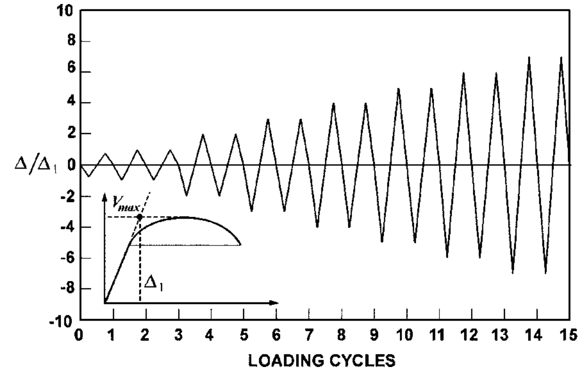

Fig. 5—Loading displacement history.

comparatively weaker section and then later extended toward the stub. Yielding of lateral steel took place during the downward movement in the 13th cycle in Specimen ASG-2NSS and in the 12th cycle in Specimen ASG-5NSS. A large amount of dilation was observed in the plastic hinge regions of all the specimens over the last few cycles before failure. During the final loading cycle, rupture of fibers in the lateral direction and buckling of longitudinal bars indicated the commencement of failure. The most damaged areas in Specimens 2NSS, 5NSS, and 7NSS were concentrated at 188, 202, and 179 mm, respectively, from the stub face.

In all the high axial load tests ($0.56P_o$), deterioration in the hinging zone was quite rapid. In almost all of the specimens, the formation of ridges started in the third cycle downward. The ridges initiated at 230 to 330 mm away from the column-stub interface. The most damaged region was concentrated at 189 to 330 mm from the stub face. First yielding of ties was observed in the 7th, 9th, and 13th loading cycles in Specimens SG-4NSS, ASG-3NSS, and ASG-6NSS that contained two, four, and six layers of GFRP, respectively. The corresponding deflections of the specimens were $2.6\Delta_1$, $4\Delta_1$, and $5.9\Delta_1$. Specimen ASGR-8NSS that was similar to ASG-6NSS but was retrofitted with six layers of GFRP after damage displayed yielding of ties in the 11th cycle at a deflection of $4.9\Delta_1$. Although all the specimens experienced flexural failure, shear effects appeared to dominate the final cycles of Specimen ASGR-8NSS. Figure 6 shows a few examples of typical damage in specimens at the end of the tests.

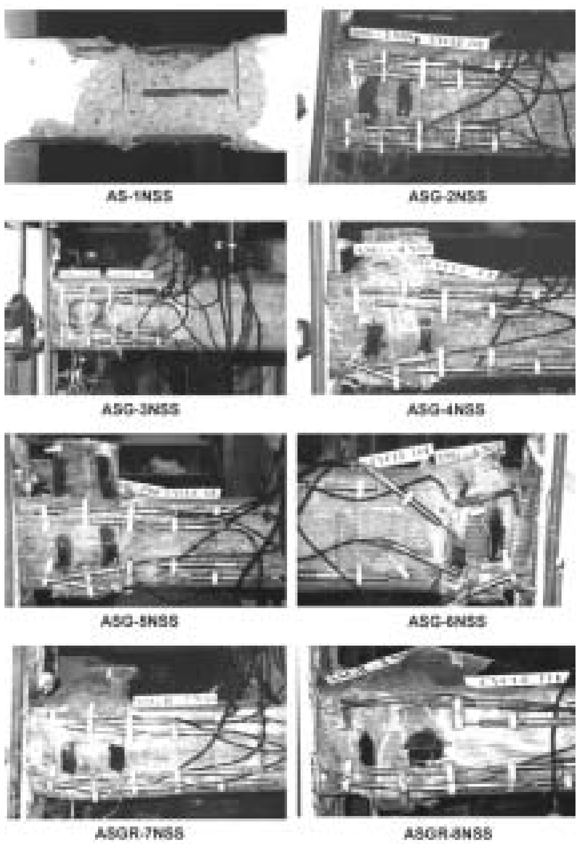

Fig. 6—Sample specimens at end of testing.

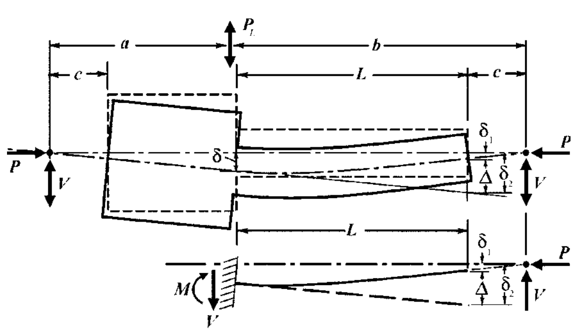

Fig. 7—Idealization of test specimens.

Analysis of results

The specimens tested in this study represented a column in a bridge or a multi-story building between the section of maximum moment and the point of inflection. Free body diagrams of the specimens are shown in Fig. 7. Behavior of a specimen can be presented in the form of applied lateral load versus stub deflection under load (P_L-δ) or shear force versus deflection at the tip of the column (V-Δ). The response of the critical section is evaluated from the moment-curvature (M-ϕ) in the most damaged zone of the plastic hinge region

The moment at a section consists of two parts, that is, primary moment caused by the lateral load and the secondary moment caused by the axial load. Deflection δ_c, used to calculate the secondary moment at the failed section, is computed from the deflected shape of column using displacements measured by vertical LVDTs located along the specimen. The curvature is calculated from the deformation readings of upper and lower LVDTs located at the most damaged regions within the hinging zone.

The values of maximum applied lateral load (P_{Lmax}), shear (V_{max}), moment (M_{max}) at the most damaged section, moment at the column-stub interface (M_{smax}), and the location of most damaged area (measured from the column-stub interface) for each specimen, are listed in Table 4. The moment-curvature response is of critical importance because deformations concentrate at the critical sections within the plastic regions during post-elastic loading and determine the column behavior. The moment-curvature responses of eight specimens tested during this study are shown in Fig. 8 to 15. Figure 16 displays the behavior of Specimen AS-1NS from a previous study[6] and is used as a control to evaluate the effects of FRP on the behavior of columns tested at lower axial loads.

Ductility parameters

In evaluating the column performance, ductility and toughness were defined using parameters as shown in Fig. 17

Table 4—Maximum forces attained during testing

Specimen	Applied axial load P/P_o	GFRP treat-ment	P_{Lmax}, kN	V_{max}, kN	M_{max}, kN·m	M_{smax}, kN·m	Most damaged zone,* mm
AS-1NSS	0.56	0 layer	310.3	105.7	167.5	195.0	458
ASG-2NSS	0.33	2 layers	372.1	126.1	226.1	250.1	188
ASG-3NSS	0.56	4 layers	363.6	123.5	230.2	252.1	207
ASG-4NSS	0.56	2 layers	346.0	118.2	219.1	232.2	189
ASG-5NSS	0.33	1 layer	354.0	120.1	223.0	235.1	202
ASG-6NSS	0.56	3 layers	391.5	132.0	265.1	285.9	204
ASGR-7NSS	0.33	2 layers	340.0	116.1	213.1	237.1	179
ASGR-8NSS	0.56	6 layers	357.0	121.1	224.5	247.5	199
AS-1NS[6]	0.33	0 layer	318.0	108.2	180.4	200.3	185
AS-3[9]	0.50	0 layer	278.5	108.8	192.9	204.0	190
AS-19[9]	0.39	0 layer	311.4	121.7	202.1	219.6	140

*Distance measured from column-stub interface to center of most damaged area.

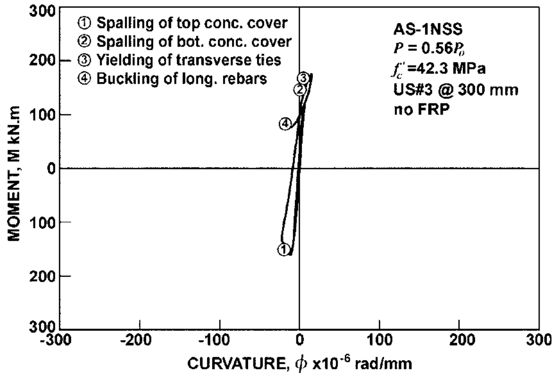

Fig. 8—Moment-versus-curvature behavior of Specimen AS-1NSS.

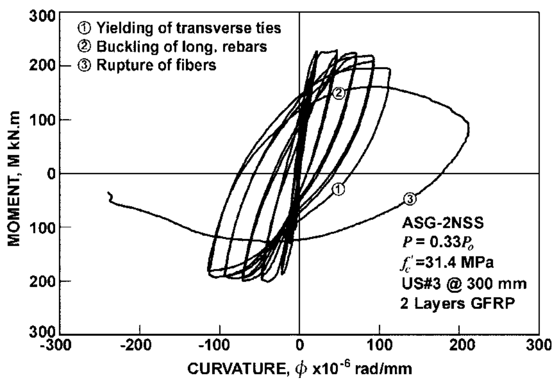

Fig. 9—Moment-versus-curvature behavior of Specimen ASG-2NSS.

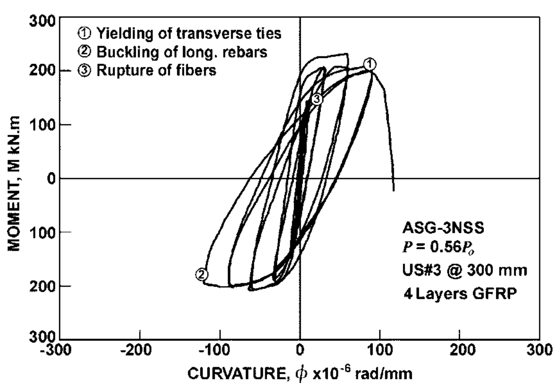

Fig. 10—Moment-versus-curvature behavior of Specimen ASG-3NSS.

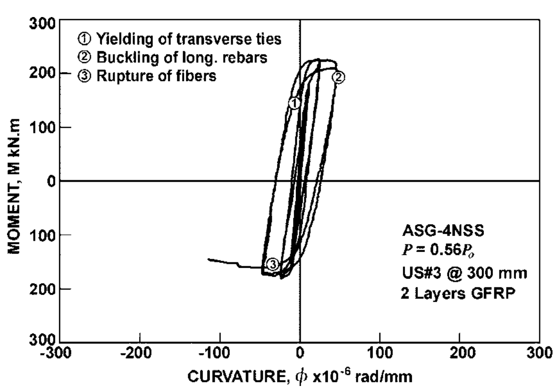

Fig. 11—Moment-versus-curvature behavior of Specimen ASG-4NSS.

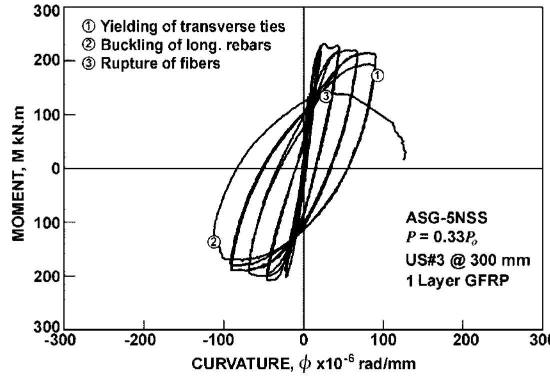

Fig. 12—Moment-versus-curvature behavior of Specimen ASG-5NSS.

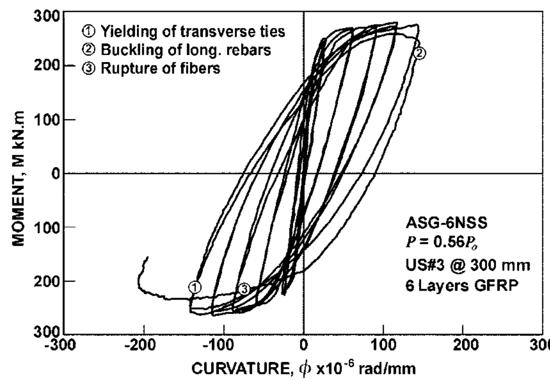

Fig. 13—Moment-versus-curvature behavior of Specimen ASG-6NSS.

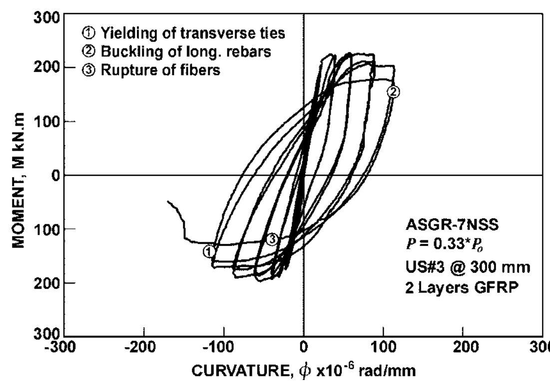

Fig. 14—Moment-versus-curvature behavior of Specimen ASG-2NSS.

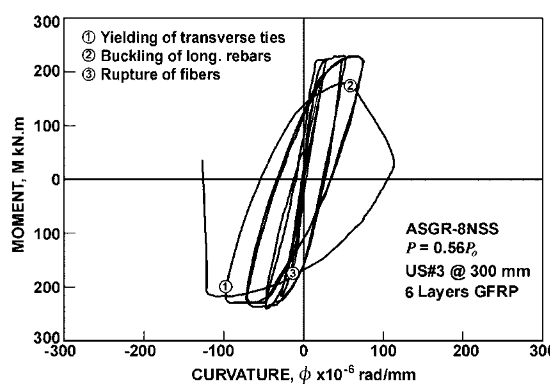

Fig. 15—Moment-versus-curvature behavior of Specimen ASG-8NSS.

and 18.[7] The curvature ductility factors (μ_ϕ) and the cumulative curvature ductility ratio (N_ϕ) represent section deformability whereas the deformation properties of the column are given by the displacement ductility factors (μ_Δ) and the cumulative displacement ductility ratio (N_Δ). The work-damage indicator (W) and energy-damage indicator (E) describe the energy dissipation capacities and toughness of an entire member and specific hinge section, respectively. Table 5 presents values for these parameters for a 10% (subscript 90) and 20% (subscript 80) reduction in moment or shear forces beyond the peak and until the end of the test (subscript t). In addition to the specimens tested during this investigation, results from some previous tests are also included in Table 5 for comparison.

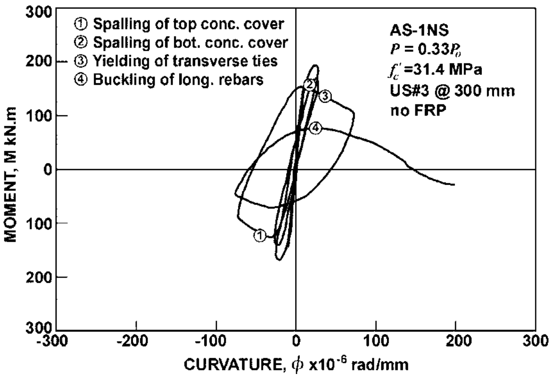

Fig. 16—Moment-versus-curvature behavior of Specimen AS-1NS.[5]

DISCUSSION OF RESULTS

Effect of GFRP retrofitting on deficient columns

To highlight the benefits of retrofitting the specimens with GFRP sheets, responses of Specimens ASG-5NSS, ASG-2NSS, and AS-1NS can be compared. Specimens ASG-5NSS and ASG-2NSS were treated with one layer and two layers of GFRP, respectively. The geometry, construction, instrumentation, and testing of these specimens were identical. All three specimens contained similar insufficient quantities of transverse steel compared with code requirements (ACI 318-02[1]) and were tested at the same level of axial load ($0.33P_o$). The only difference was their treatment with GFRP wraps. Table 5 shows the sectional and the member ductility parameters of

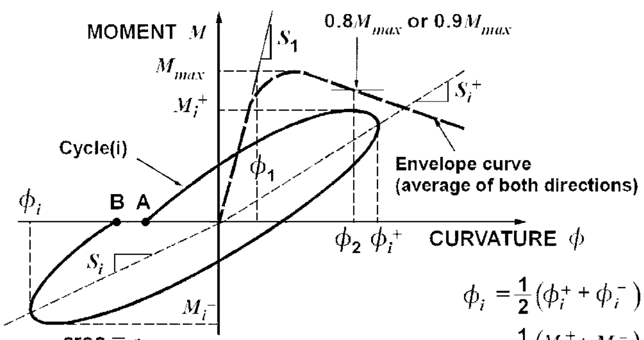

$$\phi_i = \frac{1}{2}(\phi_i^+ + \phi_i^-) \qquad M_{i,max} = \frac{1}{2}(M_i^+ + M_i^-) \qquad S_i = \frac{1}{2}(S_i^+ + S_i^-)$$

$$\mu_\phi = \frac{\phi_2}{\phi_1} \qquad N_\phi = \sum_{i=1}^{i=m} \frac{\phi_i}{\phi_1} \qquad E = \frac{1}{M_{max}\phi_1}\sum_{i=1}^{i=m} e_i \frac{L_f}{h}\left(\frac{S_i}{S_1}\right)\left(\frac{\phi_i}{\phi_1}\right)^2$$

Fig. 17—Section ductility parameters.[7]

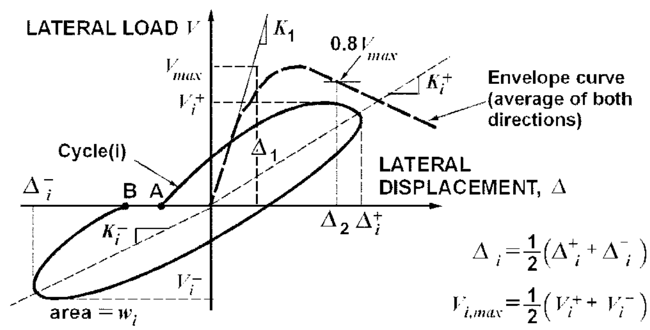

$$\Delta_i = \frac{1}{2}(\Delta_i^+ + \Delta_i^-) \qquad V_{i,max} = \frac{1}{2}(V_i^+ + V_i^-) \qquad K_i = \frac{1}{2}(K_i^+ + K_i^-)$$

$$\mu_\Delta = \frac{\Delta_2}{\Delta_1} \qquad N_\Delta = \sum_{i=1}^{i=m} \frac{\Delta_i}{\Delta_1} \qquad W = \frac{1}{V_{max}\Delta_1}\sum_{i=1}^{i=m} w_i\left(\frac{K_i}{K_1}\right)\left(\frac{\Delta_i}{\Delta_1}\right)^2$$

Fig. 18—Member ductility parameters.[7]

Table 5—Member and section ductility parameters

Specimen	Axial load, kN	f_c', MPa	GFRP treatment	Ductility factors			Ductility ratios				Energy and work-damage indicators			
				$\mu_{\phi 80}$	$\mu_{\phi 90}$	$\mu_{\Delta 80}$	$N_{\Delta 80}$	$N_{\Delta t}$	$N_{\phi 80}$	$N_{\phi t}$	W_{80}	W_t	E_{80}	W_t
AS-1NSS	$0.56P_o$	42.4	None	2.6	2.6	2.9	—	7.3	—	5.4	—	5.4	—	7.9
ASG-2NSS	$0.33P_o$	42.5	2 layers	11.5	9.0	5.9	34	58	59	79	111	241	315	450
ASG-3NSS	$0.56P_o$	42.7	4 layers	10.6	10.6	5.2	—	33	—	55	—	118	—	308
ASG-4NSS	$0.56P_o$	43.3	2 layers	7.1	7.1	4.7	15	20	—	24	40	54	—	97
ASG-5NSS	$0.33P_o$	43.7	1 layer	10.1	8.8	5.1	16	24	40	47	56	82	180	280
ASG-6NSS	$0.56P_o$	44.2	6 layers	14.7	14.7	6.8	51	87	—	135	268	565	—	945
ASGR-7NSS	$0.33P_o$	44.2	2 layers	9.1	8.2	5.0	25	35	—	54	105	200	—	256
ASGR-8NSS	$0.56P_o$	44.2	6 layers	10.3	10.3	5.1	20	28	—	49	70	95	—	280
AS-1NS[6]	$0.33P_o$	31.4	None	5.3	4.1	3.7	9.5	18.4	8.4	23.9	10.2	25.3	10.8	66.2
S-3NT[5]	$0.54P_o$	39.2	None	2.6	2.3	1.3	4.0	4.0	4.0	4.0	2.0	2.0	5.0	5.0
ST-2NT[5]	$0.54P_o$	40.4	2 layers	8.9	8.3	—	—	—	—	38	—	—	—	181
ST-4NT[5]	$0.27P_o$	44.8	1 layer	15.2	13.2	5.5	45.0	45.0	83.0	83.0	183.0	183.0	1028.0	1028.0
AS-3[9]	$0.50P_o$	33.2	None	19.0	19.0	4.7	23.0	32.0	63.0	74.0	84.0	127.0	610.0	753.0
AS-19[9]	$0.39P_o$	32.3	None	19.0	10.0	4.0	18.0	44.0	85.0	129.0	33.0	130.0	631.0	1230.0

these specimens. The benefits of GFRP retrofit can also be observed by comparing the responses of these specimens as shown in Fig. 9, 12, and 16. It can be concluded that the increase in the number of GFRP layers improves the cyclic behavior of the specimens.

Curvature ductility factors for the GFRP-wrapped specimens show improvements that range from 1.9 to 2.2 times the values for control Specimen AS-1NS. Cumulative curvature ductility ratios are also increased by a factor ranging from 1.97 to 3.3. The most significant signs of improved performance are the energy-damage indicator values. The E_{80} values increased by 17 to 29 times the values for the control specimen as a result of using FRP wraps. The moment-versus-curvature relationships show that both the strength and stiffness degradation are lower for Specimens ASG-5NSS and ASG-NSS compared with those for Specimen AS-1NS. The member ductility parameters for the wrapped specimens also show a similar trend of improved performance, compared with those for Specimen AS-1NS. Specimens ASG-2NSS and ASG-5NSS sustained 14 and 12 cycles of lateral excursions with maximum displacements of $7\Delta_1$ and $6\Delta_1$, respectively, whereas Specimen AS-1NS failed in the seventh cycle ($\Delta = 3\Delta_1$).

To evaluate the benefits of strengthening columns with GFRP wraps at high axial load ($0.56P_o$), the responses of Specimens AS-1NSS, ASG-4NSS, ASG-3NSS, and ASG-6NSS (Fig. 8, 11, 10, and 13) are compared. Specimen AS-1NSS was tested without strengthening whereas Specimens ASG-4NSS, ASG-3NSS, and ASG-6NSS were retrofitted in the test region with two, four, and six layers of GFRP, respectively. The sectional ductility parameters and member ductility parameters, shown in Table 5, clearly indicate the remarkable benefits of GFRP retrofitting scheme. The average values of curvature ductility factor for wrapped specimens are 2.8 to 5.7 times those of Specimen AS-1NSS. Similarly, the cumulative curvature ductility ratios are 4.5 to 25 times higher than those of unwrapped specimen. The most significant improvement in performance is shown by the energy damage indicator values that have increased by 12- to 120-fold as a result of GFRP wrapping. The member ductility parameters for the wrapped specimens showed a similar trend of enhanced ductile performance. Specimens ASG-4NSS, ASG-3NSS, and ASG-6NSS sustained 8, 10, and 14 cycles of lateral excursions, respectively, compared to four cycles for Specimen AS-1NSS.

The GFRP jackets also had a significant impact on maximum shear (V_{max}) and moment (M_{max}) for all strengthened specimens. Examination of shear values (Table 4) indicates that strengthened specimens attained V_{max} values that were 11 to 25% higher than the V_{max} for the control column. Similarly, retrofitted columns showed increases in M_{max} levels of 24 to 58% over control columns. It is evident that GFRP wraps mitigated the effects of large lateral steel spacing within the hinging zones and enhanced their shear and moment capacities in addition to improving ductility. The increased moment capacity of the strengthened columns may be undesirable in some cases because higher seismic forces could be transmitted to other structural elements and cause failure away from the retrofitted zone. Regardless of the number of layers, the retrofit procedure may have to include reevaluation of members such as the beam-column joints that are potential locations of failure during a seismic event.

An overview of the two sets of columns discussed above shows that the higher ductility, higher energy dissipation capacities, and enhanced shear and moment capacities were obtained through GFRP strengthening of deficient columns. Regardless of the ductility or toughness parameters considered, there was a positive relationship between improved column performance and increasing GFRP retrofit layers.

Effect of GFRP retrofitting on damaged columns

To evaluate the performance of damaged columns repaired with GFRP, the responses of Specimens ASG-2NSS and ASGR-7NSS are compared (Fig. 9 and 14). Specimen ASG-2NSS was wrapped with two layers of GFRP and tested under an axial load of $0.33P_o$, whereas Specimen ASGR-7NSS was first damaged before being retrofitted with two layers of GFRP and then tested to failure under the same level of axial load. The curvature ductility factor and cumulative curvature ductility ratios (Table 5) for Specimen ASG-2NSS are 20 and 45% higher than those for Specimen ASGR-7NSS. The energy and work damage indicator values for Specimen ASG-2NSS are 76 and 21% higher than those of the previously damaged Specimen ASGR-7NSS. The significant reduction in the total ductility parameters reflects the previous damage sustained by Specimen AS-7NS prior to retrofit. Nevertheless, considering the overall performance, the behavior of the repaired Specimen ASGR-7NSS was significantly better than that of a similar unretrofitted Specimen AS-1NS (Fig. 16).

The comparison between the responses of Specimens ASG-6NSS and ASGR-8NSS (Fig. 13 and 15) is made to evaluate the performance of a damaged column retrofitted with GFRP under higher levels of axial load ($0.56P_o$). Specimen ASG-6NSS was strengthened with six layers of GFRP before testing whereas Specimen ASGR-8NSS was first damaged then retrofitted with six layers of GFRP and finally tested to failure. Specimen ASG-6NSS sustained 14 cycles of lateral excursions compared to 11 cycles for Specimen ASGR-8NNS. The curvature ductility factor of the repaired Specimen ASGR-8NSS was 30% less than that of the strengthened Specimen ASG-6NSS. The toughness demonstrated by Specimen ASGR-8NSS, as indicated by the energy and work damage indicators, was between 17 and 30% of that of Specimen ASG-6NSS. The difference in performance between the repaired and the strengthened columns is more pronounced under high axial load ($0.56P_o$) than under low axial load ($0.33P_o$). The extent of damage prior to repair plays an important role in determining the column performance. A severe prerepair damage resulted in poor performance of the repaired column. The performance of repaired Column ASGR-8NSS, despite its extensive prerepair damage, is almost similar to that of Specimen ASG-3NSS that was strengthened with four layers of GFRP.

GFRP jacketing improves the seismic behavior of previously damaged square columns although the amount of damage sustained previously greatly affects their repair potential and salvageability. The data also indicate that a more heavily damaged column requires a higher amount of GFRP to perform in a manner similar to that of an undamaged column. The repaired specimens were seismically superior to their control unwrapped counterparts. The GFRP retrofitting techniques would be particularly useful for restoring columns that have suffered light to moderate damage during an earthquake.

Axial load effect

Effect of axial load on the seismic behavior of columns is evaluated by comparing the responses of Specimens ASG-2NSS and ASG-4NSS. Both specimens were identical in terms of the amount of lateral steel, longitudinal reinforcement, and GFRP confinement. Specimen ASG-2NSS, however, was tested at a low axial load ($0.33P_o$), whereas ASG-4NSS was tested at a high axial load ($0.56P_o$). The ductility parameters presented in Table 5 and column responses in Fig. 9 and 11 show that by increasing the axial load from $0.33P_o$ to $0.56P_o$, there is a considerable decrease in the section and member ductility. The curvature ductility factor ($\mu_{\phi 80}$) value for specimen tested at a low axial load of $0.33P_o$ (ASG-2NSS) was 11.5, which reduced to 7.1 when the axial load was increased to $0.56P_o$. Similarly, the cumulative curvature ductility ratio ($N_{\phi t}$) was reduced from 79 to 24. The energy dissipation ability also decreased very significantly. The energy dissipation for ASG-2NSS is approximately 4.7 times larger than the energy dissipated by Specimen ASG-4NSS. Similarly, the member ductility parameters are also affected by an increase in the level of axial load. The inclusion of Specimen ASG-3NSS in the comparison shows that the effects of the high axial load can be countered by an increase in the lateral FRP confinement. Specimen ASG-3NSS was strengthened with four layers of GFRP and tested at a high axial load of $0.56P_o$. Moment-curvature responses of ASG-2NSS and ASG-3NSS (Fig. 9 and 10) are very similar, with ASG-2NSS displaying a little more ductile behavior. Ultimate failure in Specimen ASG-3NSS was sudden, while Specimen ASG-2NSS failed more gradually. In all cases, and increase in axial loads adversely affected the seismic response of the columns and increased the demand on FRP jacketing. Therefore, the design procedures used to determine the amount of GFRP reinforcement required for a certain ductile performance should incorporate the effects of the axial force.

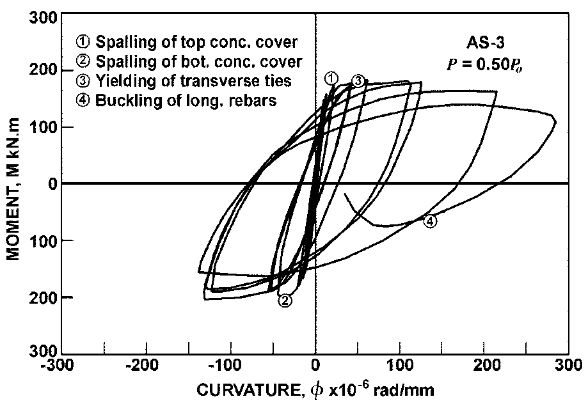

Fig. 19—Moment-versus-curvature behavior of Specimen AS-3.[9]

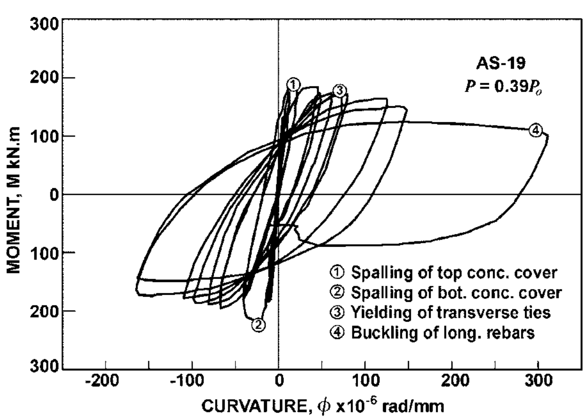

Fig. 20—Moment-versus-curvature behavior of Specimen AS-19.[9]

Stub effect

The maximum moment during testing occurred at the column-stub interface. It was observed, however, that the most damaged section was a short distance away from the stub. The column section adjacent to the interface was subjected to additional confinement provided by the stub that caused a delay in spreading cracks in concrete, and also reduced the tendency of lateral expansion at the column-stub interface. As a result, the moment capacity of the critical section increased and the failure shifted to a nearby, weaker section. For the capacity design method, this phenomenon would result in an increase in the seismic shear force in a column. Design shear should be calculated based on the actual moment capacity of the plastic hinges and their location. Similar results were obtained during the investigations[6-9] of carbon FRP-confined and steel-confined concrete columns with stubs.

Comparison with previous columns

Improvements in the behavior of columns as a result of GFRP retrofitting are particularly significant when they are compared with similar steel-reinforced columns. Specimens AS-3 and AS-19, tested by Sheikh and Khoury,[9] were designed with a sufficient amount of lateral steel as prescribed by the seismic provisions of the ACI Building Code.[1] They possessed similar material and geometric properties compared with columns of the current study. While the behavior of Specimens AS- 3 and AS-19 is shown in Fig. 19 and 20, respectively, the ductility parameters are shown in Table 5. Among specimens tested at similar low axial loads, Specimen ASG-2NSS retrofitted with two layers of GFRP displayed somewhat lower sectional ductility parameters and larger member ductility parameters than those of Specimen AS-19 (Table 5), but their overall performances were comparable (Fig. 9 and 20). A comparison of columns tested under high load levels again illustrates the benefits of the GFRP upgrades. Figure 10 and 19 show that Specimen ASG-3NSS with four GFRP layers lasted for an equivalent number of cycles as Specimen AS-3 but achieved a generally subordinate section performance. The overall member performance in both specimens was similar. Specimen ASC-6NSS with six GFRP layers (Fig. 13) exceeded the performance of code-approved Specimen AS-3 with respect to all the ductility and toughness parameters listed in Table 5. From the comparisons shown herein and reported previously, it is evident that appropriate retrofitting of deficient columns with FRP can produce responses that are superior to those of steel-reinforced columns designed for seismic resistance in accordance with the current design codes. The level of improvement observed in the strengthened specimens shows that the large number of deficient columns that exist in seismic zones could benefit from this simple rehabilitation procedure.

SUMMARY AND CONCLUSIONS

A large number of reinforced concrete columns in existing structures have inadequate confining reinforcement and can fail without sufficient warning during a major earthquake. An innovative retrofitting technique of externally bonding GFRP jackets around potential plastic regions of columns presents an efficient and economical solution for upgrading the seismic performance of such deficient columns. The research presented herein evaluates the effectiveness of strengthening deficient and repairing damaged square columns with GFRP wraps. The following conclusions can be drawn from this study:

1. Square concrete columns externally retrofitted by GFRP wraps and tested under axial compression and cyclic loading, simulating seismic loads, showed a pronounced improvement in overall sectional and member behavior over unretrofitted columns. The seismic behavior of columns represented by ductility and energy absorption capacity progressively improved through decreases in stiffness and strength degradation as the number of GFRP layers increased. Adverse effects from insufficient lateral steel are eliminated as GFRP jackets provide additional confinement to critical sections;

2. Higher ductility and improved seismic performance can be achieved by retrofitting damaged square concrete columns with GFRP jackets. The overall ductile performance, however, depends on the extent of damage sustained by the specimens prior to being wrapped. Thus, more GFRP layers are needed for highly damaged columns to achieve a performance similar to that of undamaged retrofitted columns;

3. The level of axial load has a significant effect on the overall performance of columns. A considerable reduction in ductility was observed for the specimens tested under high axial load. A larger amount of GFRP is therefore required for columns subjected to higher axial load levels to realize similar performance enhancements as those demonstrated by retrofitted columns under lower axial loads;

4. The stub attached to each column provides additional confinement thereby strengthening the column-stub interface (point of maximum moment) and shifting the failure away from stub to a section subjected to lower forces. This phenomenon requires a careful evaluation of the column shear force that can be substantially higher than that calculated by assuming the plastic hinge adjacent to the stub; and

5. The seismic behavior of deficient columns appropriately retrofitted with GFRP can be made to be superior to the response of columns having sufficient lateral steel content according to seismic provisions of the design codes.

ACKNOWLEDGMENTS

The research reported herein was supported by grants from the Natural Sciences and Engineering Research Council of Canada (NSERC) and ISIS Canada, an NSERC Network of Centers of Excellence. Additional financial assistance from Fyfe and Co., R.J. Watson Inc., and Premier Corrosion is greatly appreciated. Experimental work was carried out in the Structures Laboratories of the University of Toronto. The authors would like to express their appreciation to O. Bayrak for his assistance during the experimental work.

NOTATION

A_{ch} = cross-sectional area of structural member measured out-to-out of lateral steel
A_g = gross cross-sectional area of column
A_{sh} = total cross-sectional area of lateral steel
A_{sh} (ACI) = total cross-sectional area of lateral steel required by ACI Code
E = energy damage indicator
E_s = modulus of elasticity of steel
f_c' = compressive strength of unconfined concrete
f_{ult} = ultimate strength of steel
f_y = yield strength of longitudinal steel
f_{yh} = yield strength of lateral steel
h = column depth
L_f = length of most damaged region of column, mm
M_{max} = maximum moment at most damaged location, kN·m
M_{smax} = maximum moment at column-stub interface, kN·m
N = cumulative displacement ductility ratio
N_ϕ = cumulative curvature ductility ratio
P = applied axial load, kN
P_L = lateral load applied to columns, kN
P_{Lmax} = maximum lateral load sustained by column, kN
P_{max} = maximum axial load sustained by column, kN
P_o = unconfined theoretical axial load-carrying capacity of column, kN
s = spacing of lateral steel along axis of member, mm
V = shear force sustained by column, kN
V_{max} = maximum shear force sustained by column, kN
W = work damage indicator
Δ = lateral deflection, mm
Δ_1 = displacement corresponding to maximum lateral load along initial tangent to curve, mm
Δ_2 = displacement at section on descending portion of response curve corresponding to a certain drop in lateral load, mm
δ = deflection at column-stub interface
δ_c = deflection of column at most damaged location where moment is calculated
ε_{ult} = ultimate strain in steel
ε_y = yield strain in steel
ϕ = curvature
ϕ_1 = curvature obtained from the M-ϕ curve corresponding to maximum moment on a straight line joining origin and a point at 65% of maximum moment
ϕ_2 = curvature at section on descending portion of M-ϕ curve corresponding to a certain drop in moment
μ = ductility factor
μ_Δ = displacement ductility factor
μ_ϕ = curvature ductility factor
ρ = longitudinal steel ratio
ρ_g = ratio of area of longitudinal steel to that of cross section
ρ_s = volumetric ratio of ties to concrete core measured center-to-center of perimeter ties

REFERENCES

1. ACI Committee 318, "Building Code Requirements for Structural Concrete (ACI 318-02) and Commentary (318R-02)," American Concrete Institute, Farmington Hills, Mich., 2002, 443 pp.

2. Hall, J. F., "Northridge Earthquake of January 17, 1994, Preliminary Reconnaissance Report," *EERI Publication* No. 94-01, Earthquake Engineering Research Institute, Oakland, Calif., Mar. 1994, 104 pp

3. Comartin, C. D.; Greene, M.; and Tubbesing, S. K., "The Hyogo-Ken Nanbu Earthquake: Great Hanshin Earthquake Disaster, January 17, 1995, Preliminary Reconnaissance Report," *EERI Publication* No. 95-04, Earthquake Engineering Research Institute, Oakland, Calif., Feb. 1995, 116 pp.

4. Memon, M. S., and Sheikh, S. A., "Seismic Behaviour of Square Concrete Columns Retrofitted with Glass Fibre Reinforced Polymers (GFRP's)," *Research Report* MS0201, Department of Civil Engineering, University of Toronto, Toronto, Ontario, Canada, Sept. 2002.

5. Sheikh, S. A., and Yau, G., "Seismic Behavior of Concrete Columns Confined with Steel and Fiber-Reinforced Polymers," *ACI Structural Journal*, V. 99, No. 1, Jan.-Feb. 2002, pp. 72-80.

6. Iacobucci, R. D.; Sheikh, S. A.; and Bayrak, O, "Retrofit of Square Concrete Columns with Carbon Fiber-Reinforced Polymer for Seismic Resistance," *ACI Structural Journal*, V. 100, No. 6, Nov.-Dec. 2003, pp. 785-794

7. Sheikh, S. A., and Khoury, S., "A Performance-Based Approach for the Design of Confining Steel in Tied Columns," *ACI Structural Journal*, V. 94, No. 4, July-Aug. 1997, pp. 421-431.

8. Bayrak, O., and Sheikh, S. A., "High-Strength Concrete Columns under Simulated Earthquake Loading," *ACI Structural Journal*, V. 94, No. 6, Nov.-Dec. 1997, pp. 708-722.

9. Sheikh, S. A., and Khoury, S., "Confined Concrete Columns with Stubs," *ACI Structural Journal*, V. 90, No. 4, July-Aug. 1993, pp. 414-431.